High-Transparency, Self-Standable Gel-SLIPS Fabricated by a Facile Nanoscale Phase Separation

Issei Okada and Seimei Shiratori*

School of Integrated Design Engineering, Keio University, 3-14-1 Hiyoshi, Kohoku-ku, Yokohama, Kanagawa 223-8522, Japan

Ⓢ Supporting Information

ABSTRACT: Slippery liquid-infused porous surfaces (SLIPSs) that were both highly transparent and free-standing (self-standability) were fabricated by an extremely simple process using non-solvent-induced phase separation (NIPS) of a poly(vinylidene fluoride-co-hexafluoropropylene) (PVDF-HFP)/di-n-butyl phthalate solution. We call these "Gel-SLIPS" because the porous PVDF-HFP film fabricated using the NIPS process has been used as a gel electrolyte in a lithium-ion battery. In previous reports, SLIPS fabrication required complex processes, high annealing temperatures, and drying. Gel-SLIPS can be fabricated from the adjusted solution and the lubricant at room temperature and pressure in 5 min by squeegee, cast, or dip methods. NIPS is based on a quick phase separation process in situ, and reduction of the surface energy is not required because of the considerable fluorine in PVDF-HFP. Moreover, because of the flexible nanonetwork structure of PVDF-HFP, Gel-SLIPS exhibited self-standability and high transmittance (>87% at 600 nm). Gel-SLIPS is thus highly versatile in terms of the fabrication process and film characteristics.

KEYWORDS: SLIPS, PVDF-HFP, DBP, NIPS method, wet process, transparent, self-standing
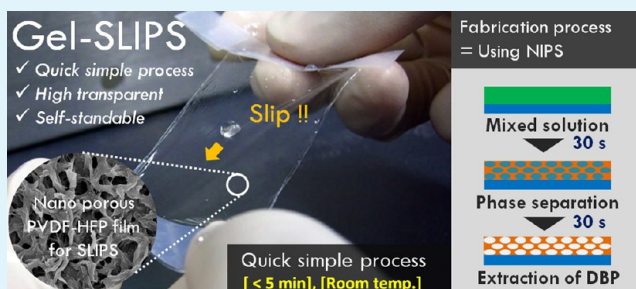
1. INTRODUCTION

Antifouling surfaces are highly desirable for solar cells, automobiles, medical devices, fuel transport, buildings, food containers, and many other objects. A new type of antifouling surface, slippery liquid-infused porous surfaces (SLIPS), was recently reported[1] that is a low-energy microporous surface infused by a liquid lubricant. SLIPS exhibits antiwetting against almost all fluids and is stable at high temperature and pressure because of lubricant in the porous structure. While antiwetting surfaces inspired by the lotus-leaf effect have been studied for decades,[2-14] it is extremely difficult to achieve stability against low-surface-tension liquids, drop impact, and extreme temperatures and pressures.[15-17] Therefore, SLIPS is highly attractive, and there are various fabrication methods. However, those methods are not very versatile, as evidenced by the following reports.

Wong et al.[1] used a poly(tetrafluoroethylene) (PTFE) mesh and an epoxy resin array as a rough surface to accommodate the lubricant. PTFE mesh has minimal formability, so it cannot be applied to the surface of complex structures. Moreover, it is not transparent in the visible region. Meanwhile, an epoxy resin array surface is fabricated by a complex, time-consuming, two-step soft-lithography process.[18,19] These fabrication processes are neither versatile nor suitable for mass production. Other complex, lengthy, and high-cost processes include photo-lithography, deep reactive ion etching, and chemical vapor deposition.[20,21] In contrast, for rough surfaces, a more cost-effective and simpler SLIPS fabrication process involving alumina sol−gel was reported by Ma et al.[22] This was a simple

wet process, and the fabricated layer had high transmittance in the visible. However, it required annealing at high temperature (400 °C) and a reduction of the surface energy, which caused limitations in substrate selectivity, as well as increased costs because of the extra steps and materials. Other fabrication methods with similar issues include boehmite treatment for aluminum,[23,24] alkaline etching of copper,[25] and electrolytic polymerization of polypyrrole.[26] In summary, high versatility, high transparency, and formability are needed for SLIPS fabrication, but previous fabrication methods were complex and time-consuming and the substrate selectivity was limited.

In this study, a porous poly(vinylidene fluoride-co-hexafluoropropylene) (PVDF-HFP) film was fabricated by non-solvent-induced phase separation (NIPS), which is a very simple process based on self-organized phase separation that is complete in several minutes under ambient temperature and pressure. Moreover, because PVDF-HFP has a high fluorine content with an initially low surface energy, it does not require additional reduction of the surface energy. Hence, the combination of NIPS and PVDF-HFP is a simple fabrication process providing rough surface structures and a low-surface-energy film for SLIPS. Previously, we fabricated "Gel-SLIPS" for "electrolyte gelation" of lithium-ion batteries.[27,28] However, the optimum film structure for SLIPS is completely different from that of electrolyte gelation. The film structure for gel
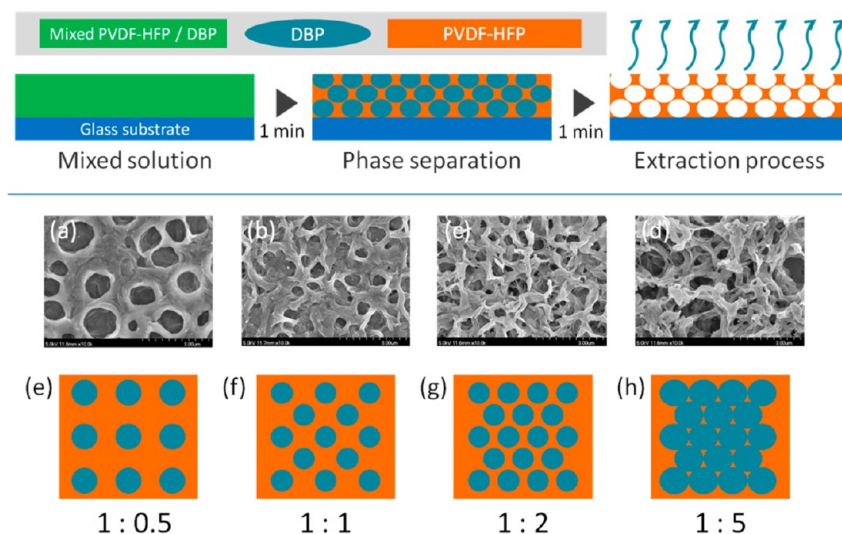
Figure 1. (Upper part) Phase separation and extraction process (NIPS method). (a−d) SEM images of PVDF-HFP film surfaces for initial PVDF-HFP/DBP weight ratios of (a) 1:0.5, (b) 1:1, (c) 1:2, and (d) 1:5, respectively. Every magnification was 10000×. (e−f) Simple phase-separation models of (e) 1:0.5, (f) 1:1, (g) 1:2, and (h) 1:5, respectively.

electrolytes is optimized for high mobility of electrolyte ions, whereas the SLIPS film structure requires a rough surface for retaining the lubricant. Here, the gelation electrolyte process was applied for SLIPS, and the optimum Gel-SLIPS film structure was determined by changing the ratio of the additive in the phase separation. Moreover, we desired high transmittance and self-standability to maximize high versatility.

2. EXPERIMENTAL SECTION

2.1. Materials. Poly(vinylidene fluoride-*co*-hexafluoropropylene) (PVDF-HFP; $M_w \sim 400000$, $M_n \sim 130000$), which has a 10 mol % ratio of HFP to VDF, was purchased from Aldrich (St Louis, MO). The reason why we adopted PVDF-HFP was that it has both solubility to acetone and a low surface energy. Di-*n*-butyl phthalate (DBP; 99.5%), acetone (99.5%), and ethanol (99.5%) were purchased from Kanto Chemical (Tokyo, Japan). Glass was used as a substrate (Micro slide glass s 1226, refractive index =1.52, Matsunami, Osaka, Japan). Perfluoropolyether (PFPE; Krytox 103, DuPont, Wilmington, DE) was used as a lubricant.

2.2. Adjustment of a PVDF-HFP/DBP Solution. PVDF-HFP and DBP were added to acetone at a concentration of 20 wt %, and the weight ratio of PVDF-HFP/DBP was varied (1:0.5, 1:1, 1:2, and 1:5) as a parameter for controlling the film structure based on phase separation between PVDF-HFP and DBP. The solution was stirred for 1 h at 50 °C and subsequently aged for >24 h at room temperature.

2.3. Fabrication of a Nanoporous PVDF-HFP Film. The PVDF-HFP/DBP solution was spread onto a glass substrate by a simple, wet squeegee method at ambient conditions. The squeegee condition was that the gap made by two pieces of mending tape (thickness = 0.058 mm) purchased by Sumitomo 3M (Tokyo, Japan) was 0.058 mm. Therefore, the solution volume on the glass substrate was 5.8 mm³ per 1.0 cm². The PVDF-HFP/DBP layer was dried for >1 min at room temperature, during which phase separation of PVDF-HFP and DBP naturally proceeded. In the dried PVDF-HFP/DBP layer, the structure based on phase separation was fixed. The layer was immersed in ethanol for >1 min to extract DBP and blown with air for 10 s, yielding a pure, porous PVDF-HFP film.

2.4. Fabrication of Gel-SLIPS. PFPE lubricant was infused into the PVDF-HFP porous film, which initially seemed translucent but then became transparent with infused PFPE. The PFPE-infused PVDF-HFP film on glass was then blown with air to remove excess PFPE.

2.5. Characterization Measurements. The surface morphologies of the PVDF-HFP porous films were investigated with a field-emission scanning electron microscopy (FE-SEM; S-4700, Hitachi Ltd., Tokyo, Japan). The thickness and surface roughness were determined with a laser microscope (VK-9700 Generation II, KEYENCE, Osaka, Japan). Sliding angles were measured using contact-angle meters (CA-DT, Kyowa, Saitama, Japan). The transmittance was measured using ultraviolet−visible absorption spectroscopy (UV-mini 1240, Shimadzu, Japan). The photocurrent density−voltage curves of single-crystal standard solar cells (CIC, Yamaguchi, Japan) were measured under illumination with an AM 1.5 solar simulator (100 mW cm^{-2}) for a 2.8-cm² masked area. A 500-W xenon lamp (UXL-500SX, Ushio Inc., Tokyo, Japan) was used as the light source. The mechanical strength and flexibility (extension rate) were determined with a tensile strength tester (EZ-LX, Shimadzu, Kyoto, Japan). The samples for the tensile strength test were 20 × 60 mm and 2 μm thick.

3. RESULTS AND DISCUSSION

3.1. Surface Morphologies of PVDF-HFP Films. SLIPS requires a high-roughness surface to retain the lubricant. Here, suitably rough surface PVDF-HFP films were determined by changing the PVDF-HFP/DBP ratio during the NIPS process. Figure 1 (upper part) schematically depicts the simple NIPS method. Initially, PVDF-HFP and DBP phase separate. Subsequently, DBP is extracted from the PVDF-HFP/DBP layer, yielding a porous PVDF-HFP film with a rough surface. The number of pores and their sizes determine the surface roughness and can be changed by varying the amount of DBP in the mixture. Thus, the critical parameter for the surface roughness is the PVDF-HFP/DBP ratio. Parts a−d of Figure 1 show SEM images of PVDF-HFP film surfaces for various PVDF-HFP/DBP ratios. We refer to the samples by their ratios; e.g., the film for a PVDF-HFP/DBP ratio of 1:0.5 is "1:0.5". In Figure 1a−d, only 1:0.5 exhibited a surface morphology composed of both pores and flat areas, while the 1:1, 1:2, and 1:5 structures had networks of pores and fibers. The respective film structures are understood in terms of the simple two-dimensional phase separations given in Figure 1e−h. We refer to the previous report,[29] which examined more about NIPS. There is no report on the combination of PVDF-HFP and DBP; however, a basic theoretical model for NIPS was explained in detail in the report. In the case of our study (PVDF-HFP and DBP), when 1:0.5 and 1:1 are compared, the

extra DBP increased the pore density and reduced the flat surface area. Therefore, the surface area of 1:1 seemed fiberlike rather than flat. For 1:2, the density of the pores increased relative to 1:1, as shown in Figure 1f,g, causing decreased fiber diameters, as shown in Figure 1b,c. Finally, when comparing 1:5 and 1:2, we see that the pore size increased but the fiber diameter hardly changed in Figure 1c,d, indicating that, because the pores were connected, the pore sizes rather than the density of the pores increased, as depicted in Figure 1g,h. Thus, initially increasing the amount of DBP increased the density of the pores, while further increases of DBP connected the pores, increasing their size. For a discussion about the pore size and fiber diameter through all samples, as shown in Figure 2, the
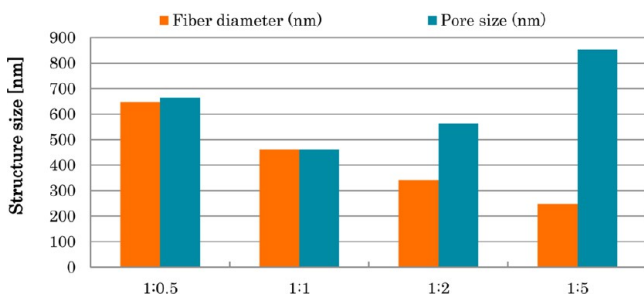
Figure 2. Fiber diameters and pore sizes that were measured from SEM images, which are an average of eight measurement points.

tendency was found. As for the fiber diameter, it decreased with increasing DBP ratio. As for the pore size, except for the 1:0.5 sample, it increased with increasing DBP ratio. The reason why the pore size of 1:0.5 was bigger than 1:1 was that 1:1 had some ampule structure pores, which seemed to be dark pores. The ampule structure has a small opening and a spacious internal space. Hence, the film that has ampule structure seems to have small pore size. The ampule structure was made when DBP droplets came to rise toward the surface of the wet film [because the density of DBP (1.05 g/cm^3) is less than that of PVDF-HFP (1.78 g/cm^3)] and were fixed before perfectly going out of the film. The possibility that DBP droplets were fixed at the middle of going out of film is lower than 1:1 because 1:0.5 has a smaller amount of DBP than 1:1. Therefore, 1:1 had more ampule structure than 1:0.5 and the pore size of 1:1 seemed smaller than that of 1:0.5. As shown in Figure 3, the
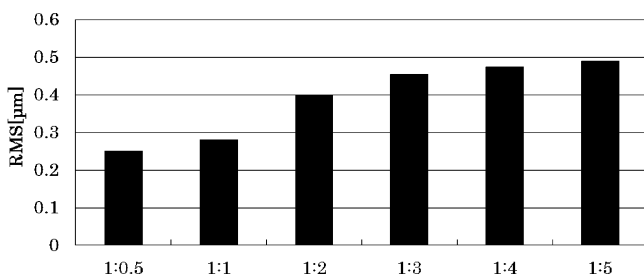
Figure 3. rms surface roughness of the PVDF-HFP film.

root-mean-square (rms) roughness increased with increasing DBP through all samples. The surface roughness of the films is one of the most important factors for SLIPS. At the transition between 1:1 and 1:2, the difference was larger than that among 1:2, 1:3, 1:4, and 1:5. For clarification of the differences among samples, 1:5 was chosen as the representative of one of the parameters. Therefore, in this study, 1:0.5, 1:1, 1:2, and 1:5 are

used as representatives of the parameters. Figure 4 shows the PVDF-HFP film thicknesses. The film thicknesses of 1:0.5, 1:1,
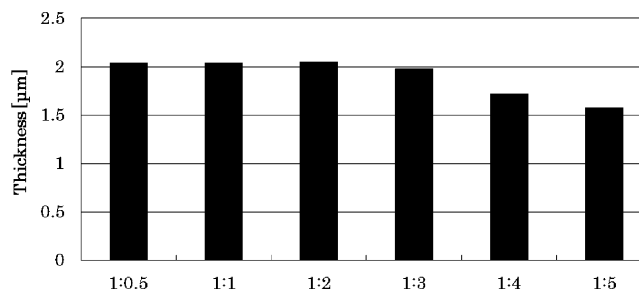
Figure 4. Thickness of the PVDF-HFP film.

1:2, and 1:3 were almost the same, while that of 1:4 was thinner and that of 1:5 was much thinner. From 1:0.5 to 1:3, the reason why the thickness hardly changed was that increasing DBP led to higher porosity. On the other hand, from 1:3 to 1:5, increasing DBP additionally led to decreasing thickness because of the excessive amount of DBP. Therefore, a PVDF-HFP film that had a PVDF-HFP:DBP ratio >1:4 should have been more fragile. The Mechanical Strength and Flexibility are discussed below.

3.2. Sliding Angle on Gel-SLIPS. As reported by Kim et al.,[23] the surface morphology of the film affects the retention of lubricant: rough surfaces retain the lubricant while flat surfaces do not. Figure 5 shows the sliding angles of water and oleic acid
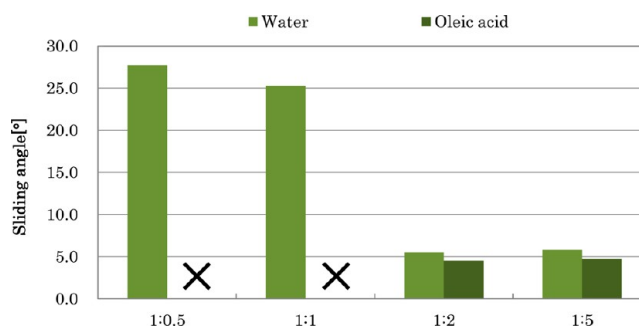
Figure 5. Sliding angles of water and oleic acid on Gel-SLIPS ("×" represents the sticking of the liquid to the surface).

on Gel-SLIPS. The surface energies of water and oleic acid are 72.2 and 32.0 mN/m, respectively. Both water and oleic acid exhibited sufficiently low sliding angles for 1:2 and 1:5, while for 1:0.5 and 1:1, the higher sliding angles indicated sticking to the surface. Figure 6 shows a model for sticking the liquid to the surface. Parts a and b of Figure 1 show that 1:0.5 and 1:1 had flat PVDF-HFP surface areas and lower surface roughness relative to those of 1:2 and 1:5. Therefore, 1:0.5 and 1:1 did not have suitable structures for retaining the lubricant. Because flat areas in particular were not able to retain the lubricant, the liquid was caught by an exposed flat area like that illustrated in the upper part of Figure 6. On the other hand, because 1:2 and 1:5 had few flat surface areas and sticking points, as shown in the lower part of Figure 6, they exhibited low sliding angles for water and oleic acid. Moreover, 1:2 and 1:5 was enable to slide a hexane droplet, the surface energy of which was much lower (18.4 mN/m). Sliding angles of 1:2 and 1:5 against hexane were 3.4° and 3.6°, respectively. Therefore, Gel-SLIPS also showed the possibility of sliding various liquids. In summary,
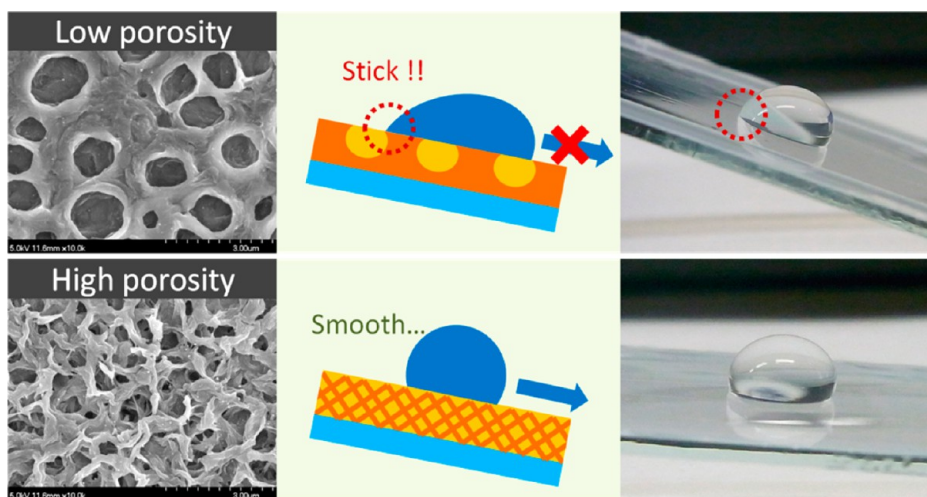
Figure 6. Models depicting why a liquid sticks or slides smoothly.

we were able to observe adequately low sliding angles for Gel-SLIPS using 1:2 and 1:5 PVDF-HFP films.

3.3. Transparency of Gel-SLIPS. Considering the wide range of applications (e.g., antifouling layers for solar cells and windows), SLIPS should have high transparency in addition to simple processing. Figure 7 shows the transparency in the
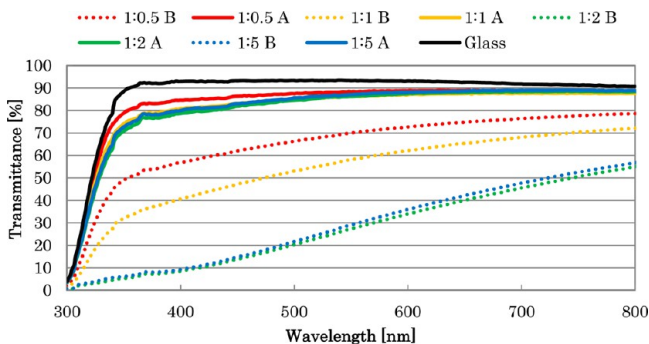

Figure 7. Transmittance of PVDF-HFP films after (solid lines, A) and before (dashed lines, B) infusion with a PFPE lubricant.

visible region of a PVDF-HFP film before and after infusion with a lubricant. All of the PVDF-HFP films prior to lubricant infusion had <80% transmittance for the whole visible region (>400 nm), whereas after infusion, they exhibited roughly 80% transmittance in the visible region. Following lubricant infusion, all of the PVDF-HFP films exhibited roughly 88% transmittance at 600 nm (to within 2%), despite the large differences in transmittance prior to infusion (Figure 8). Figure 9 depicts a model for why transmittance improved after infusion with a PFPE lubricant. Before infusion, the optical path was a network structure of PVDF-HFP and air, whose refractive indices are 1.40 and 1.00, respectively. In contrast, after infusion, the optical path was a network structure of PVDF-HFP and a PFPE lubricant with refractive indices of 1.40 and 1.29, respectively. Thus, the infused PVDF-HFP layer had smaller differences in the refractive index. The reflectance of an interface between two materials is related to the refractive indices of the two materials, as given by eq 1. (For simplicity, the dependence on the incident angle is ignored.)
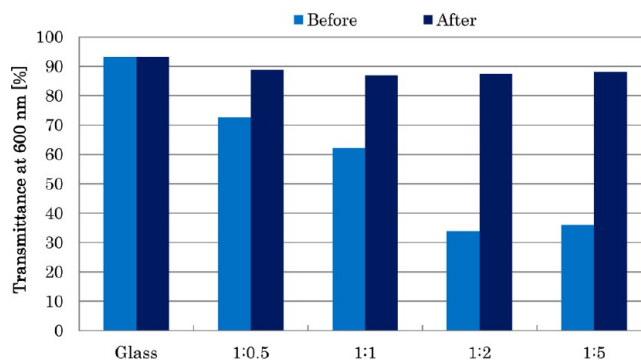

Figure 8. Transmittance at 600 nm for PVDF-HFP films before and after infusion with a PFPE lubricant.
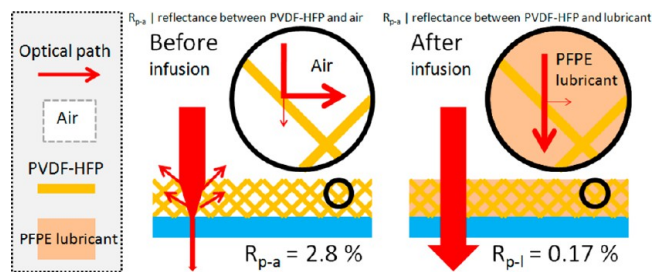

Figure 9. Model for why transmittance improved after infusion with a PFPE lubricant.

$$R_{a-b} = \left(\frac{n_a - n_b}{n_a + n_b} \right)^2 \qquad (1)$$

R_{a-b} represents the reflectance of the interface between a and b, with refractive indices n_a and n_b, respectively. For the PVDF-HFP/air and PVDF-HFP/PFPE interfaces, R_{p-a} and R_{p-l} are 2.8% and 0.17%, respectively. In the model depicted in Figure 9, every PVDF-HFP fiber reflects the incident light with 2.8% or 0.17% reflectance. Therefore, before infusion, the PVDF-HFP film induced irregular reflections that decreased the overall transmittance, while the infused film induced far fewer irregular reflections and exhibited higher transmittance. Upon comparison of the glass substrate and Gel-SLIPS (the PVDF-HFP film after lubricant infusion), the difference in transmittance was roughly 5% and Gel-SLIPS was highly trans-

parent, as shown in Figure 13. However, if the network size of the film was reduced to <100 nm and the diffraction at the PVDF-HFP and PFPE lubricant interfaces was ignored, the transmittance of Gel-SLIPS from eq 1 becomes 93.45% with the air/lubricant, lubricant/glass, and glass/air interfaces. Therefore, we predict that the transmittance of Gel-SLIPS could be improved by a smaller network structure of the film.

We applied Gel-SLIPS on solar cells and compared the performance with that of bare cells. Figure 10 plots the
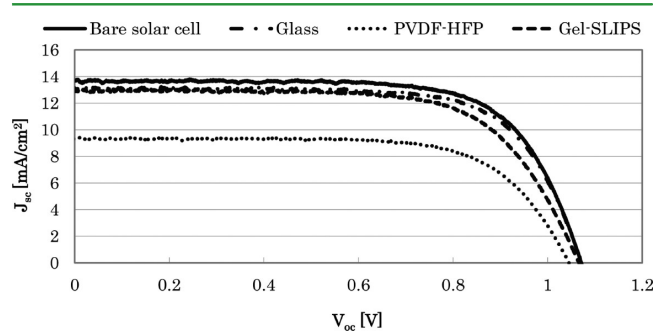
Figure 10. Photocurrent density (J_{sc}) versus voltage (V_{oc}) for a bare solar cell, one covered with a glass substrate (Glass), one covered with a PVDF-HFP film (prior to infusion) on glass (PVDF-HFP), and one covered with Gel-SLIPS on glass (Gel-SLIPS), respectively.

photocurrent density (J_{sc}) versus voltage curves (V_{oc}) of a bare solar cell, a cell covered with a glass substrate (glass), a cell covered with a PVDF-HFP film on a glass substrate prior to infusion (PVDF-HFP), and a solar cell covered with Gel-SLIPS on a glass substrate (Gel-SLIPS). We used 1:2 for the PVDF-HFP film because it exhibited low sliding, high transmittance, and self-standability (discussed below). Only PVDF-HFP caused a significant decrease in the solar cell performance, while the others exhibited small differences. These results match the decreased range of transmittance shown in Figures 7 and 8. Table 1 summarizes the solar cell results. While PVDF-

Table 1. Summary of the Photovoltaic Performance of Solar Cells under Various Conditions (See the Text and Figure 10 for Details)

	V_{oc} [V]	J_{sc} [mA/cm^2]	FF	η [%]
bare solar cell	1.073	13.722	0.701	10.323
glass	1.073	13.093	0.705	9.898
PVDF-HFP	1.058	9.337	0.684	6.751
Gel-SLIPS	1.066	12.934	0.677	9.333

HFP exhibited a significant decrease (−3.572%) in the conversion efficiency (η) relative to the bare solar cell, Gel-SLIPS exhibited a small decrease (0.990%). Relative to the bare glass (glass), the decrease in the conversion efficiency was −0.565%. Because Gel-SLIPS can be directly fabricated on the solar cells without a glass substrate, the actual decrease of the conversion efficiency is −0.565%. Thus, Gel-SLIPS is a promising antifouling layer for the solar cell.

3.4. Mechanical Strength and Flexibility. Gel-SLIPS exhibited self-standability (i.e., free-standing ability), which had never been reported for SLIPS. It was peeled off a glass substrate by initially attaching a piece of tape to the noninfused lubricant part of Gel-SLIPS and lifting the tape. Gel-SLIPS was peeled off of the glass substrate simultaneously. We examined the tensile strength and extension rate with the tensile strength

tester because self-standability is a result of both the tensile strength and flexibility. Figure 11 plots the tensile strength of
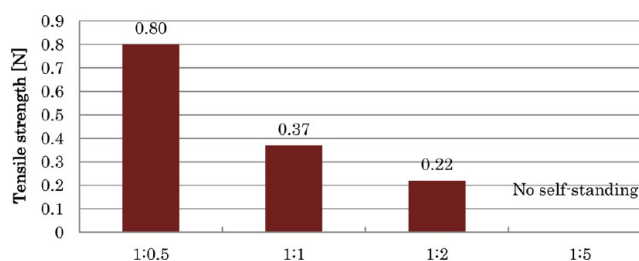
Figure 11. Tensile strengths of Gel-SLIPS self-standing films.

the self-standing Gel-SLIPS film for 1:0.5, 1:1, and 1:2 (1:5 did not produce a free-standing film). The tensile strength was reduced with increasing DBP because the network density of the PVDF-HFP film decreased, as observed in Figure 1a−d. The lowest tensile strength was 0.22 N.

Figure 12 shows extension rates of more than 168% for the self-standing Gel-SLIPS films, indicating significant flexibility.
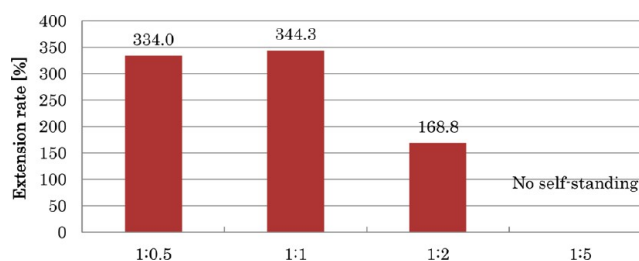

Figure 12. Extension rates of Gel-SLIPS self-standing films.

Because Gel-SLIPSs are self-standing (see Figure 13), they can be used as sticker SLIPSs, which are suitable for disposable SLIPSs. A sticker SLIPS, however, cannot be attached to a complex object. Therefore, the cast method was developed. Figure 14 shows a Gel-SLIPS fabricated on a rounded glass lens by casting the PVDF-HFP/DBP solution on the glass, followed by the same procedures documented above. If the object is flexible and bent, Gel-SLIPS may be durable because of its own flexibility. Thus, Gel-SLIPS is fabricated not only by the squeegee method but also by the cast method and by the dip method. The formability of a Gel-SLIPS film is therefore extremely good because of its flexibility and versatile fabrication methods.

4. CONCLUSIONS

By controlling the NIPS process with the PVDF-HFP:DBP ratio, Gel-SLIPS were successfully fabricated by an extremely simple process with a fabrication time of less than 5 min under ambient conditions. Moreover, Gel-SLIPS can be fabricated with a variety of methods (squeegee, cast, and dip) on various substrates with high formability. The NIPS method is effective because it is based on a quick, self-assembled, nanophase separation process in situ, and reduction of the surface energy is not required because of the considerable fluorine content in PVDF-HFP. Characterization of Gel-SLIPS indicated that the 1:2 sample exhibited a low sliding angle against water (5.5°) and oleic acid (4.5°), a high transmittance (87.44% at 600 nm of wavelength), and self-standability. Therefore, 1:2 is an optimal ratio for a versatile SLIPS. Because of their tensile
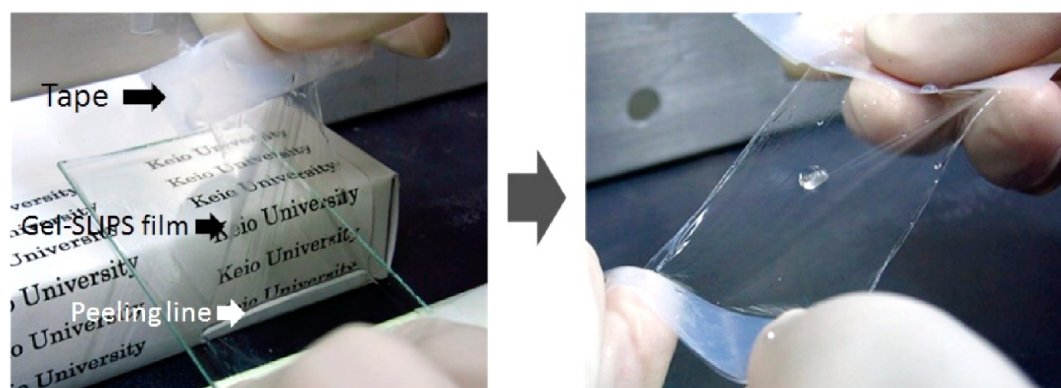
Figure 13. (Left) Photograph of the peeling off a self-standing Gel-SLIPS from a glass substrate. The self-standing process movie is given as movie 3 in the Supporting Information. (Right) Water droplet on the self-standing Gel-SLIPS, given as movie 4 in the Supporting Information.
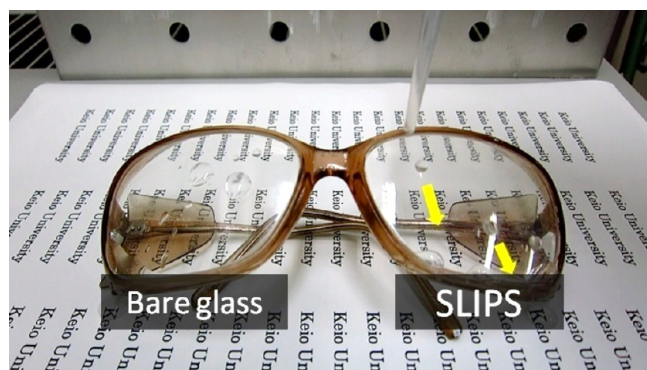
Figure 14. Gel-SLIPS fabricated with the cast method on a round glass surface. Yellow arrows mean the sliding direction of the water droplets. This is given as movie 1 in the Supporting Information.

strength, flexibility, and transparency, SLIPS films were produced that were clear and self-standing. In addition, by its high formability, a round glass surface could be coated. In summary, transparent and self-standing Gel-SLPSs were prepared by a quick and highly formable fabrication process, making them highly versatile for numerous applications.

■ ASSOCIATED CONTENT

Ⓢ Supporting Information

Movies showing that a water droplet is sliding on the goggle surface covered with Gel-SLIPS (left, bare surface; right, surface covered by Gel-SLIPS; movie 1), showing that a oleic acid droplet is sliding on the goggle surface covered with Gel-SLIPS (left, bare surface; right, surface covered by Gel-SLIPS; movie 2), showing the self-standing process (in other words, the Gel-SLIPS film is being peeled off from a glass substrate; movie 3), showing the self-standing Gel-SLIPS film and the moving water droplet on the film (movie 4), and showing resistance against scratching with a finger wearing a glove (movie 5). This material is available free of charge via the Internet at http://pubs.acs.org.

■ AUTHOR INFORMATION

Corresponding Author
*E-mail: shiratori@appi.keio.jp.

Notes
The authors declare no competing financial interest.

■ REFERENCES

(1) Wong, T.-S.; Kang, S. H.; Tang, S. K. Y.; Smythe, E. J.; Hatton, B. D.; Grinthal, A.; Aizenberg, J. *Nature* **2011**, *477*, 443−447.
(2) Barthlott, W.; Neinhuis, C. *Planta* **1997**, *202*, 1−8.
(3) Herminghaus, S. *Europhys. Lett.* **2000**, *52*, 165−170.
(4) Sun, T.; Feng, L.; Gao, X.; Jiang, L. *Acc. Chem. Res.* **2005**, *38*, 644−652.
(5) Quere, D. *Rep. Prog. Phys.* **2005**, *68*, 2495−2532.
(6) Artus, G. R. J.; Jung, S.; Zimmermann, J.; Gautschi, H.-P.; Marquardt, K.; Seeger, S. *Adv. Mater.* **2006**, *18*, 2758−2762.
(7) van der Wal, P.; Steiner, U. *Soft Matter* **2007**, *3*, 426−429.
(8) Chiou, N.-r.; Lu, C.; Guan, J.; Lee, L. J.; Epstein, A. J. *Nat. Nanotechnol.* **2007**, *2*, 354−357.
(9) Tuteja, A.; Choi, W.; Ma, M.; Mabry, J. M.; Mazzella, S. A.; Rutledge, G. C.; McKinley, G. H.; Cohen, R. E. *Science* **2007**, *318*, 1618−1622.
(10) Yuan, J.; Liu, X.; Akbulut, O.; Hu, J.; Suib, S. L.; Kong, J.; Stellacci, F. *Nat. Nanotechnol.* **2008**, *3*, 332−336.
(11) Tuteja, A.; Choi, W.; Mabry, J. M.; McKinley, G. H.; Cohen, R. E. *Proc. Natl. Acad. Sci. U.S.A.* **2008**, *105*, 18200−18205.
(12) Deng, X.; Mammen, L.; Butt, H.-J.r.; Vollmer, D. *Science* **2012**, *335*, 67−70.
(13) Ebert, D.; Bhushan, B. *Langmuir* **2012**, *28*, 11391−11399.
(14) Park, K.-C.; Choi, H. J.; Chang, C.-H.; Cohen, R. E.; McKinley, G. H.; Barbastathis, G. *ACS Nano* **2012**, *6*, 3789−3799.
(15) Lafuma, A.; Quere, D. *Nat. Mater.* **2003**, *2*, 457−460.
(16) Liu, Y.; Chen, X.; Xin, J. H. *J. Mater. Chem.* **2009**, *19*, 5602−5611.
(17) Nguyen, T. P. N.; Brunet, P.; Coffinier, Y.; Boukherroub, R. Q. *Langmuir* **2010**, *26* (23), 18369−18373.
(18) Pokroy, B.; Epstein, A. K.; Persson-Gulda, M. C. M.; Aizenberg, J. *Adv. Mater.* **2009**, *21*, 463−469.
(19) Stone, H. A. *ACS Nano* **2012**, *6*, 6536−6540.
(20) Anand, S.; Paxson, A. T.; Dhiman, R.; Smith, J. D.; Varanasi, K. K. *ACS Nano* **2012**, *6*, 10122−10129.
(21) Rykaczewski, K.; Anand, S.; Subramanyam, S. B.; Varanasi, K. K. *Langmuir* **2013**, *29*, 5230−5238.
(22) Ma, W.; Higaki, Y.; Otsuka, H.; Takahara, A. *Chem. Commun.* **2013**, *49*, 597−599.
(23) Kim, P.; Kreder, M. J.; Alvarenga, J.; Aizenberg, J. *Nano Lett.* **2013**, *13*, 1793−1799.
(24) Wilson, P. W.; Lu, W.; Xu, H.; Kim, P.; Kreder, M. J.; Alvarenga, J.; Aizenberg, J. *Phys. Chem. Chem. Phys.* **2013**, *15*, 581−585.
(25) Xiao, R.; Miljkovic, N.; Enright, R.; Wang, E. N. *Sci. Rep.* **2013**, *3*, 1988.
(26) Kim, P.; Won, T.-S.; Albarenga, J.; Kreder, M. J.; Adorno-Martinez, W. E.; Aizenberg, J. *ACS Nano* **2012**, *6*, 6569−6577.
(27) Choi, J.-W.; Kim, J.-H.; Cheruvally, G.; Ahn, J.-H.; Kim, K.-W.; Ahn, H.-J.; Kim, J.-U. *J. Ind. Eng. Chem.* **2006**, *12*, 939−949.

1507

dx.doi.org/10.1021/am404077h | *ACS Appl. Mater. Interfaces* 2014, 6, 1502−1508

(28) Cao, J.-H.; Zhu, B.-K.; Xu, Y.-Y. *J. Membr. Sci.* **2006**, *281*, 446−453.

(29) Gregory, R.; Guillen, Y. P.; Minghua, L.; Eric, M. V. H. *Eng. Chem. Res.* **2011**, *50*, 3798−3817.